Journal of Colloid and Interface Science **227,** 334–344 (2000)
doi:10.1006/jcis.2000.6899, available online at http://www.idealibrary.com on IDEAL®

Adsorption and Exchange Dynamics in Aging Hydroxyethylcellulose Layers on Silica

Ervin Mubarekyan and Maria M. Santore[1]

Department of Chemical Engineering, Lehigh University, 111 Research Drive, Bethlehem, Pennsylvania 18015

Received August 20, 1999; accepted April 10, 2000

The adsorption kinetics of hydroxyethylcellulose (HEC) on silica and relaxations in adsorbed HEC layers were probed using total internal reflectance fluorescence and near-Brewster reflectivity. Like many random-coil polymers, HEC was found to adsorb at the transport-limited rate. Relaxations occurred at nearly constant interfacial mass when HEC layers were exposed to aqueous solvent, causing the subsequent exchange of chains between the layer and the free solution to become increasingly hindered. Eventually, on the time scale of a day, layers became immobilized and unable to accommodate chains from free solution. A continued fluorescence decay, beyond time scales that could be probed with self exchange, suggested further relaxations of the adsorbed HEC. The polydisperse HEC system (with an average molecular weight near 450,000) behaved qualitatively similar to molecular weight standard polyethylene oxide (PEO) layers on silica. For instance, relaxations in PEO layers occurred on a time scale of 10–20 h, like the HEC layers. Young layers of the latter, however, exhibited self-exchange kinetics that were an order of magnitude slower than PEO layers of similar age. This difference in adsorbed layer dynamics was attributed to HEC's stiffer backbone, compared with flexible PEO.

Key Words: **adsorbed layer relaxations; self-exchange kinetics; polydisperse layers; segment–surface contacts; layer mobility.**

INTRODUCTION

Polymers are added to colloidal dispersions in a variety of technologies to control dispersion stability and mediate rheology. In addition to the choice of polymer chemistry and architecture to ensure the ultimate stabilization or flocculation for a particular system, processing time scales and shear conditions can be critical in achieving the desired dispersion performance.

The thickness of polymer layers adsorbed on colloidal particles is established at least as fast as the adsorbed amount (1); however, other layer properties continue to evolve on longer time scales (2). An adsorbed layer's hydrodynamics depend on the outermost region of the layer, the tails in the case of adsorbed homopolymers (3). The tails are also responsible for long-range colloidal interactions (4–6); therefore, the initial attractions or repulsions between particles would be expected to develop on time scales similar to that for hydrodynamic development.

If flocculation occurs, the floc density and the ultimate sediment properties such as the compactness of a filter cake are influenced not by the individual layer thicknesses (tails), but by dynamic features of the originally adsorbed polymers (7). These include concentrated polymer solution dynamics (8), made more complicated by the effects of polymer chain adhesion to the colloidal particles. Segment–surface contacts evolve on longer time scales than the initial mass accumulation and, in some instances, have been shown to be essentially irreversible, making parts of the adsorbed layer glass-like (9). The development of segment–surface interactions can also influence the formulation characteristics of stable dispersions by controlling the rate of chain translation between an interface and bulk solution (10, 11), as additional components are added to the formulations or as conditions such as solvent quality or temperature are changed.

Our work on adsorbed layer relaxations was motivated by the current lack of quantitative understanding and questions about the universality of previously observed behavior. For instance, Frantz found initially exponential displacement of protiopolystyrene on silica by deuteriopolystyrene in cyclohexane (11, 12). Conversely, with displacement of preadsorbed protiopolystyrene by polymethyl methacrylate, stretched exponential kinetics were observed (13). Based on observations of exponential displacement of protiopolystyrene by deuterio-*cis*-polyisoprene at high temperatures (14) and stretched exponential kinetics for the same system at low temperatures (15), it was argued that exponential behavior should be expected near local equilibrium, with stretched exponential kinetics coming into play for systems exhibiting a diffusive kinetic barrier to exchange. In contrast with these studies, a close quantitative analysis of polyethylene oxide (PEO) self-exchange on silica revealed kinetics that were neither exponential nor stretched exponential (10). Also of interest, the PEO system ultimately relaxed to yield populations of chains physically adsorbed to the silica, but which appeared permanently tethered on experimental time scales. The size of the immobile population increased with molecular weight (10).

The current work explores the extent to which some of the previous observations about adsorbed layer relaxations hold

[1] To whom correspondence should be addressed.

0021-9797/00 $35.00

for practical polymer additives such as hydroxyethylcellulose (HEC). For instance, the observed molecular weight dependence of polystyrene layer relaxations (11, 12) suggests that interpreting relaxations in HEC layers would be challenging: HEC is polydisperse, and our attempts at fractionation failed. Despite the complexity, one might still expect to draw some conclusions about HEC, since prior studies with PEO layers revealed only a weak dependence of the apparent equilibration time on molecular weight (10). Interestingly, the individual self-exchange traces with PEO depended more on molecular weight than did the overall relaxation times. We were therefore interested to learn, with HEC, if a similar apparent equilibration time would be found and if the self-exchange times would be system specific. Additionally, from a comparison of HEC and PEO relaxation behavior, we hoped to gain insight into the relative roles of backbone stiffness and segment–surface interaction of adsorbed layer dynamics. While the steric hindrance parameter, σ, a dimensionless measure of the thermodynamic backbone stiffness (16), is 1.9 for HEC and 1.4 for PEO (16, 17), the two polymers have similar segment–surface interactions with silica in aqueous solution. The ether linkages in the polymers undergo hydrogen bonding with surface silanols, contributing about 2.5 kT each (18). This estimate was derived from van der Beek's displacement calculation method (19), using other data in the literature (20, 21). Additionally for HEC adsorption onto silica, it has been suggested that hydroxyls from the polymer may interact with dissociated silanols (22, 23). This contribution to HEC adsorption is, however, thought to be minor because Tadros showed very weak adsorption of polyvinyl alcohol (PVA) to silica (24). Our own experiences have also shown negligible adsorption of dextran to glass. The hydrogen bonding between hydroxyls on the polymer and dissociated surface silanols at neutral pHs appears to be a minor energetic contribution to HEC adsorption, suggesting that the ether–silanol hydrogen bonds are dominant for PEO and HEC adsorption on silica.

In this paper, we first explore the adsorption kinetics of HEC on silica to characterize the basic adsorption behavior of this system. Results are compared with expectations for transport-limited behavior, and free solution diffusion coefficients are compared with those in the literature. The framework for self-exchange experiments with HEC is then established. To this end, the proportionality between the fluorescence signal in the TIRF (total internal reflectance fluorescence) study is evaluated: Fluorescence is shown to be proportional to the adsorbed amount of labeled chains, after a correction is made for contributions from the bulk solution, which is orders of magnitude more concentrated than in our prior studies. We also found that with the HEC system, a fluorescence decay spontaneously occurs after adsorption, even though the surface mass is constant. This is attributed to slow relaxations and reconfigurations of the adsorbed chains. Finally, the extent to which fluorescent tagging alters the adsorption is evaluated. Self-exchange studies are then interpreted in the context of a reversible first-order exchange model to reveal the underlying surface constants. It is shown that a first-order reversible self-exchange model including transport resistances predicts exponential self-exchange kinetics in tracer studies where the labels do not shift the equilibrium.

EXPERIMENTAL

Silica surfaces, generated by acid treatment of soda lime glass microscope slides (Fisher Finest), were used as the adsorption substrates. The glass slides comprised one wall of a thin-slit flow channel, 1.3 or 0.4 mm deep for reflectivity or TIRF studies, respectively. The silica surface was generated by filling the flow cell with concentrated sulfuric acid for 15 h, flushing with DI (deionized) water, and finally flowing pH 7.4 phosphate buffer prior to each experiment (25). Adsorption studies were conducted by pumping polymer solutions through the laminar shear flow cell at wall shear rates ranging from 3 to 30 s^{-1}, sufficiently gentle to avoid distorting the polymer chains or altering the fundamental adsorption kinetics. The continuous flow was necessary to establish local concentration gradients and distinguish free solution diffusion from surface-dominated processes.

HEC (Natrosol GR) was a gift from Aqualon. Our GPC analysis, using a series of PEO standards to calibrate the column, revealed an equivalent weight-averaged molecular weight of 440,000 and a polydispersity of 5.3. The sample's degree of substitution was reported by Aqualon to be between 2.1 and 2.5, indicating that substantial amounts of unreacted hydroxyl groups remained on the cellulose backbone. Also of note for this degree of substitution, Brown reports that some of the ethoxy side groups are converted to small polyethylene oxide oligomers, containing multiple ether linkages (26).

The HEC was randomly labeled with fluorescein isothiocyanate isomer I (Aldrich) via isothiocyanate chemistry. The reaction was conducted in dimethylformamide for 24 h at 100–110°C under argon with an iron(III) acetylacetonate catalyst (18). Products were precipitated from solution by acetone or ethyl acetate, in which the catalyst and excess dye remained dissolved. The labeled FHEC was then purified by successive dissolution in DI water and precipitation by acetone until negligible free dye was detected in the supernatant. The final product contained 2.3 mol FITC/100,000 g HEC, determined by absorbance at 488 nm. (Note that, with the reaction carried out in a good solvent for both the polymer and the label, with attachment of the fluorescein to remaining backbone hydroxyls, and with this low level of labeling along the polymer backbone, we have no reason to expect blocky label addition to the backbone.) Labeled samples were stored as dry powders to prevent degradation. Adsorption experiments were carried out in dilute phosphate buffer (0.008 M Na_2HPO_4 and 0.002 M KH_2PO_4) to fix the pH at 7.4. The emission spectrum of FITC is highly pH sensitive, and the phosphate buffer minimizes the quantum yield reduction that occurs as labeled polymer adsorbs on an acidic silica surface (27).

Adsorption, exchange, and desorption kinetics at the center of the glass flat were studied by a combination of near-Brewster

optical reflectivity and TIRF. The TIRF experiments employed an argon ion laser at 488 nm with photon counting detection, as previously described (27–29). Near-Brewster reflectivity studies employed a helium neon laser at 633 nm and single element or array photodiode detectors. The calibration procedures for both techniques have been discussed previously (25, 27–29). In the current work with randomly labeled FHEC, the fluorescent signal should be proportional to the adsorbed mass of labeled HEC. The near-Brewster technique also returns the adsorbed mass. Therefore, TIRF and reflectivity should return the same kinetic traces in studies where all material is labeled.

RESULTS AND DISCUSSION

Static Coverage Levels

Adsorption isotherms provide information about the relative coverage levels of adsorbed polymers and may approximate equilibrium partitioning of a polymer between a solution and an interface (though there are questions whether equilibrium is truly achieved). Isotherm shapes also potentially provide insight into the adsorption mechanism or expected layer morphology. The isotherm for HEC on silica, measured by near-Brewster reflectivity, is shown in Fig. 1. The coverage levels, on the order of 0.4–0.5 mg/m^2, are reminiscent of those previously found for PEO on silica (25) and consistent with the idea that HEC layers follow the classic tail–loop–train structure (30). While these data are shown for unlabeled HEC, we found no difference in the coverages for the tagged FHEC. The free solution concentrations in Fig. 1 are plotted on a logarithmic scale, and each datum represents a run in which the polymer solution was continuously pumped over the silica surface for a time well beyond that needed for saturation. (The actual times for each datum were widely varied because the adsorption time is roughly proportional to the free solution concentration.) The continuous flow maintains the bulk polymer concentration at its original level, eliminating the need for separations and assays that contribute to uncertainty in the free polymer concentration.

The most notable feature about Fig. 1 is the flatness of the isotherm, extending down to a free solution concentration of 0.5 ppm. Flat isotherms (with plateaus extending down to concentrations many orders below a ppm) are expected for monodisperse high-molecular-weight homopolymers with moderate segment–surface attractions and reversible physisorption (31). Frequently, adsorption isotherms done in batch mode have curved shapes, and low coverages are measured for dilute free solution concentrations as a result of polydispersity (32) or difficulties separating polymer-bearing particles from the solution and assaying the latter (33, 34). Because the HEC is polydisperse (on the order of 5), the relatively flat shape in Fig. 1 may come as a surprise, but could stem from prolonged continuous flow of fresh polymer solution. Since the late stages of an adsorption run involve the displacement of short chains by long ones, with long chains dominating the surface at long times, the coverages in Fig. 1 may correspond to adsorption of the longer populations within the polydisperse solution.

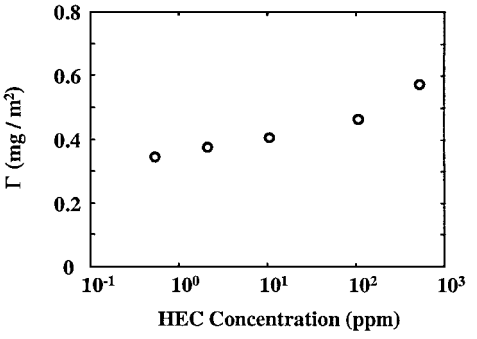

FIG. 1. The surface coverage of HEC as a function of its bulk concentration.

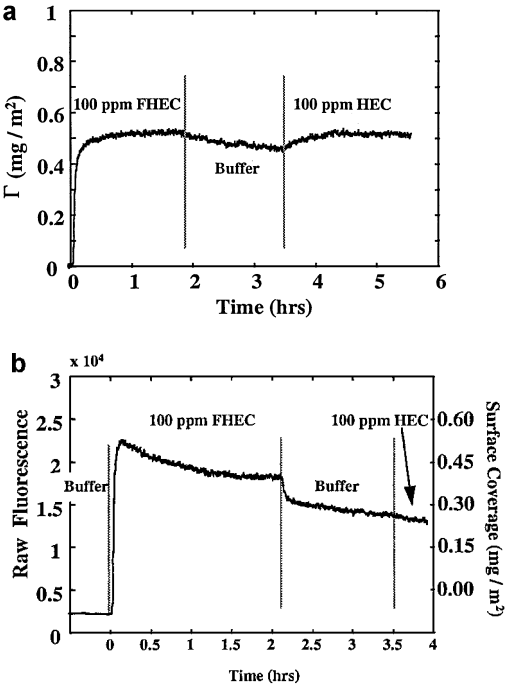

FIG. 2. Adsorption of 100 ppm FHEC onto silica and subsequent exposure of the layer to buffer and then 100 ppm native HEC (a) monitored by reflectivity, (b) monitored by TIRF. In part (b), the right axis refers to the surface excess during the adsorption process and does not include the free fluorescein contribution to the signal. Since about 350 of the total fluorescence counts come from free fluorescein, the first 350 counts of raw fluorescence are not counted toward the surface coverage. Also since the fluorescence signal changes slowly in response to layer relaxations, the right axis pertains only to the initial adsorption part of the curve.

Adsorption Kinetics

In addition to quantifying the general features of adsorption and desorption kinetics, this section discusses an important issue best addressed in the context of dynamic studies: the linearity of the TIRF calibration.

General features of adsorption and desorption kinetics. Figure 2 compares reflectivity and TIRF traces during a typical adsorption run, in this case for a bulk solution concentration

of 100 ppm. In Fig. 2a, the reflectivity experiment is conducted at a wall shear rate of $5\,s^{-1}$. Initially there is buffer flowing through the cell and, upon a valve turnover, the FHEC solution enters the cell at time zero. The signal begins to rise as the adsorption begins, and there is a substantial linear adsorption regime before the surface coverage rounds a shoulder and levels off. Close examination of Fig. 2a reveals that, following the shoulder, there is a very slight increase in the surface coverage even an hour into the run. This round shoulder and subsequent gradual increase are most likely a result of polydispersity. Adsorption of narrow PEO molecular weight standards gave a linear signal rise, a sharp turnover, and a flatter signal once the surface was saturated (10). In the case of polydisperse FHEC, the surface initially adsorbs all chains diffusing from solution. Once saturated, however, long chains are likely to continue to adsorb, displacing shorter chains. The equilibrium coverage for long homopolymer chains is generally greater than that for short chains of the same chemistry, giving rise to the increasing signal at long times.

In Fig. 2a, after 2 h flowing the 100 ppm FHEC solution, the buffer was pumped through the cell. During the subsequent 2 h, very little FHEC was desorbed, only $0.05\ mg/m^2$. This observation is consistent with the isotherm in Fig. 1. Fully saturated coverage levels coexist near equilibrium with dilute free solutions of 0.5 ppm or less, providing minimal driving force for desorption. The most rapid desorption rate possible (the diffusion limited case) will be one where the driving force for chain diffusion from the surface is the concentration in solution near the surface (read from the isotherm) minus the vanishing bulk solution concentration (35). This concentration driving force is a fraction of a ppm. Therefore, whenever isotherms like those in Fig. 1 are measured, with a flat plateau down to dilute bulk solution concentrations, desorption will persist at time scales slower than can be reasonably measured.

In Fig. 2a, after about 1.5 h of flowing buffer, a 100 ppm solution of unlabeled HEC is injected. The signal rises slowly as the overall coverage approaches its previous level. This time, however, the HEC chains needed to make up the ultimate coverage adsorb more slowly than the initial FHEC adsorption, because the surface is very nearly saturated at the time of HEC injection. The observation that the ultimate HEC coverage is similar to that of the originally adsorbed FHEC suggests minimal influence of fluorescent tagging on adsorption.

Figure 2b shows the TIRF trace for the adsorption sequence in Fig. 2a. Because of necessary differences in the TIRF and reflectivity cells, the wall shear rate in TIRF experiments was $20\,s^{-1}$, compared to $5\,s^{-1}$ in Fig. 2a. The wall shear rate will have, at most, a 1/3-power influence kinetics when surface processes are rapid. The same general kinetic features should therefore appear in both traces of Fig. 2.

Figure 2b starts with kinetics similar to Fig. 2a: Adsorption is initially rapid. Near surface saturation in the TIRF run, however, the signal passes through an overshoot and continues to slowly decay over the next several hours, never quite leveling off. After 2 h for FHEC adsorption, buffer is injected and causes a rapid signal decrease. This decrease, on the order of the cell residence time, occurs because the flowing buffer removes free FHEC from the solution in the evanescent zone. (Figure 2a confirms that none of the rapid signal drop is due to desorption.) In Fig. 2b, the slower subsequent decay during buffer flow is due to a combination of chain relaxations and desorption. (The decreasing part of the overshoot during FHEC flow is also attributed to relaxations, as discussed two sections below.) Finally, after 11/2 h of buffer flow, unlabeled HEC is injected and there is a very slight increase in the signal decay rate, signaling minimal displacement of labeled chains by unlabeled chains in this particular example. Because of the complexities in Fig. 2b, both the raw fluorescence signal and an estimated surface coverage, applicable only to the early-stage kinetics and not to the long-time fluorescence decay, are shown on the y axis.

Control studies confirmed that photobleaching did not contribute to the fluorescent signal evolution. This possibility was ruled out by tracking fluorescent decays for 16 h in two separate runs. In the first, the FHEC layer was continuously illuminated and in the second, the layer was illuminated occasionally to check the fluorescence. Both decays were identical.

Quantification of initial adsorption kinetics. Most polymers with affinity for a substrate adsorb quickly, such that the initially observed rate corresponds to the diffusion limit. Our studies confirm that this is indeed the case for HEC adsorption. Furthermore, the consistency of the TIRF and reflectivity data in describing the initial adsorption kinetics confirm that over short periods of time (where slow processes like layer relaxations are minimal), the fluorescence is linear in the adsorbed amount.

Leveque solved the convection–diffusion equation (which applies to our adsorption cell) with a boundary condition of instantaneous adsorption on the glass flat, giving a local free polymer concentration of zero at all times (36). This situation persists in experiments having fast adsorption and a surface whose capacity is sufficiently large that the concentration gradient in free solution reaches steady state. Then a constant transport-limited adsorption rate, $d\Gamma/dt$ depends only on the free solution concentration, C, the wall shear rate, γ, and the bulk solution diffusion coefficient, D, according to

$$\frac{d\Gamma}{dt} = \frac{1}{\Gamma(4/3)9^{1/3}}\left(\frac{\gamma}{DL_\infty}\right)^{1/3} DC. \qquad [1]$$

L_∞ is the distance from the entrance port to the point of observation.

All our adsorption traces exhibited linear kinetics up to 90% of the total coverage, at which point a shoulder or overshoot set in for reflectivity or TIRF, respectively. The initial adsorption rate was directly proportional to the free solution concentration, per Eq. [1], and the scaling of the adsorption rate on the wall shear rate to the 1/3 power was also confirmed, suggesting transport-limited adsorption. The linearity of the TIRF and reflectivity traces during initial adsorption also demonstrates a direct proportionality between interfacial fluorescence and

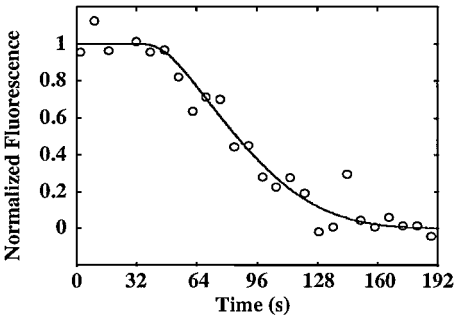

FIG. 3. Convection–diffusion model fit (curve) to experimental TIRF data (circles) for a nonadsorbing surface from which HEC chains are diffusing away. This particular fit yields $D = 5.7 \times 10^8$ cm^2/s.

adsorbed mass. This proportionality was used as a basis for calibrating the fluorescence signal, in Fig. 2b (keeping in mind that the free chain fluorescence doesn't contribute to the adsorbed mass). The total coverage and the ultimate time to approach full surface coverage (the onset of the shoulder in reflectivity runs) were also found to be consistent with transport limited behavior in Eq. [1].

While it is useful to solve the convection–diffusion equation with an adsorbing boundary condition, as Leveque and others have done, solution of the same equation with a nonadsorbing impenetrable surface facilitates calculation of the evolving free solution concentration near the glass surface as the cell is filled or emptied with fluorescent material (37). Such cell filling traces have been previously described quantitatively by Lok (38) and in dimensionless form depend on Reynold's and Peclet's numbers, the latter containing the free solution diffusivity. Therefore, measurements of interfacial fluorescence during cell filling or emptying facilitate an independent measurement of the diffusivity (37).

In Fig. 3 we fit the numerically generated solution of Lok's equations (38) to fluorescence traces of free FHEC being flushed from the cell, for instance, the kinetic feature occurring near 2 h in Fig. 2b. During the short time of cell flushing, the fluorescence from the layer forms a constant background which is subtracted prior to the fit, and the remaining signal from the free polymer is normalized to unity. A diffusion coefficient, $4–5 \times 10^{-8}$ cm^2/s, was obtained by averaging the results of several similar experiments. This value, which is slightly slower than others reported for Natrosol GR based on dynamic light scattering (9×10^{-8} cm^2/s for a sample whose MW was reported to be 500,000) (26), corresponds to a diffusion-averaged hydrodynamic coil diameter of 48 nm (following Navier–Stokes). Differences may be due to the different HEC batches and details of the molecular weight distribution. (Notably, when this procedure was used for narrow molecular weight standard PEO samples, the diffusivity was in good agreement with values obtained by other methods (25).) When our HEC diffusivity value was employed in Eq. [1], the expected adsorption rates were in good quantitative agreement with the initial time evolution of the reflectivity signal. This confirms both transport-limited initial adsorption, up to 90% coverage, and the validity of the optics-based calibration methods (25) for the reflectivity technique.

Relaxations and fluorescein quantum yield. The fluorescence during the first 90+% of all adsorption traces was proportional to the adsorbed mass, indicating a nearly constant interfacial fluorescein quantum yield during initial adsorption. Comparison of the TIRF and reflectivity data in Fig. 2 demonstrates that, after saturation, the fluorescence signal continues to evolve while the mass does not, signaling a sensitivity of fluorescence to secondary changes within the layer. In Fig. 2b, the fluorescence signal decays 20% in about 2 h, as FHEC solution flows. During subsequent exposure to flowing buffer, the fluorescence continued to decay to a greater extent than could be explained by the desorption of 0.5 mg/m^2 of FHEC. We believe that, in Fig. 2b, the fluorescence decay resulted from layer relaxations, especially during the prolonged contact with FHEC solution. During the subsequent buffer flow, both relaxations and desorption contribute to the decay.

There are two routes by which the fluorescence signal could decrease in response to interfacial relaxations: First, movement of the labels within the evanescent field (all other things constant) could alter the fluorescence. For instance, if the layer relaxed in such a way that the tags moved away from the surface, the fluorescence signal would decrease by 13% for each 10 nm of average tag motion for a 80-nm evanescent wave. That relaxations would cause the labels to move away from the surface is, however, unlikely. As chains reconfigure there are probably increased numbers of trains, bringing the fluorophores closer, on average, to the surface. Thus, the second (and more likely) mechanism for the decay is that the quantum yield is reduced when polymer relaxations bring the fluorescein labels closer to the surface.

The local pH near a silica surface is lower than that of a neutral bulk solution. Fluorescein is highly pH sensitive with a pK_a near 6.8 and quenching under acidic conditions. These two effects, together, can be used as a basis for an interfacial pH sensor (27) or as a measure of molecular reconfiguration, as Robeson has shown (39). For a silica surface with a potential of -200 mV, a bulk solution pH near 7, an ionic strength of 0.028 (the current work), the model in Ref. (27) predicts that, as labels move from a distance of 20 to 15 nm away from the interface, the fluorescence decreases by 3%. (This calculation accounts for the quantum yield and evanescent wave intensity changes.) However, were the fluorophores to be displaced 5 nm, moving from 10 to 5 nm from the surface, the fluorescence would decrease $\sim$50%. Therefore, a net nanometer-scale movement of the fluorophores about the interface, especially those originally between 5 and 10 nm from the surface, can substantially change the fluorescence. Because the incremental change in the quantum yield is nonlinear in interfacial distance, we will not pursue further quantification of the effect in this paper.

It is noteworthy that the fluorescence overshoot in Fig. 2b differs from overshoots previously observed with fluorescein-tagged PEO. In samples containing mixtures of

fluorescein-tagged and unlabeled PEO, the latter displaced the former after initial adsorption, causing a signal decrease. Adsorption of unlabeled PEO on silica is preferred over fluorescein-tagged PEO because the latter bears two negative charges for each fluorescein, which are electrostatically repelled from the silica. In the case of HEC adsorption, the electrostatic repulsion is potentially present; however, no dramatic increase in the severity of the overshoot was observed when unlabeled HEC was deliberately added to FHEC. One obvious reason for the lack of the labeling effect in the current study is the higher ionic strength which reduces the electrostatic range. Therefore, in the work presented here, we do not attribute the reduction in fluorescence signal to displacement of labeled chains by those bearing fewer labels per unit mass.

Self-Exchange Dynamics and Layer Relaxations

Shortly after their initial adhesion to a surface, chains will still be configured in a manner similar to their shape in free solution. With time, however, adsorbed chains relax to increase their segment–surface contacts and entanglements, a process in which we are interested. While the fluorescence quenching from the previous section provides one measure of chain relaxation, the fluorescence evolution may not be linearly proportional to a convenient layer property (for instance, the average segment–surface separation). While we do know that as long as the fluorescence evolves so does the layer, we would also like to understand the nature of the relaxations and their impact on layer properties. To this end, we performed self-exchange studies. In a self-exchange experiment, one preadsorbs a layer of labeled or unlabeled chains and, after a specified period, exposes the adsorbed layer to unlabeled or labeled chains, respectively, which displace those that have adsorbed previously. The kinetics of the exchange process provide insight into the dynamic state of the layer, interfacial populations with differing tightnesses of binding, and the overall aging process of the adsorbed layer.

When interpreting self-exchange experiments, one must keep in mind that self-exchange traces are but one measure of adsorbed layer relaxations. As the layer age prior to the initiation of self-exchange is increased, the shapes of a series of self-exchange traces should converge to a single shape, characteristic of the relaxed layer. Even after the convergence of the self-exchange series, however, the layer might continue to evolve in a way that is detectable only by other measures. Further, if the layer appears immobile in a self-exchange study (i.e., the challenging chains are unable, on a reasonable experimental time scale, to displace those previously adsorbed), this does not mean that the layer is done evolving. Subsequent slow rearrangements within the layer may not be detectable with self-exchange. Finally, while we intended to use self-exchange as a means to probe the process of layer aging, the test is far from perfect. To trace some aspect of an aging polymer layer, one should employ a method that provides a snapshot of the layer at different ages, or at least, the time needed to run the test should be an order of magnitude shorter than the layer age at the time of testing. This is not always the case with self-exchange experiments which, themselves, can be rather sluggish. Therefore, when interpreting self-exchange kinetics as a measure of layer aging, we placed the most emphasis on the short-time-exchange kinetics. The longer time self-exchange kinetics were measured and reported to provide additional perspective, keeping the limitations of the experimental strategy in mind.

Quantitative interpretation of self-exchange kinetics relies on a model in which the invading chains diffuse from the bulk solution to the interface with mass transfer coefficient M and undergo a first-order reversible self-exchange reaction on the surface, and the displaced chains diffuse away from the interface with the same mass transfer coefficient, M (since the diffusivities of the labeled and unlabeled chains should be identical). The surface exchange reaction depends on forward and reverse kinetic rate constants k_{ex} and k'_{ex}

$$\theta_{FHEC} + HEC \underset{k'_{ex}}{\overset{k_{ex}}{\Leftrightarrow}} \theta_{HEC} + FHEC. \qquad [2]$$

Here, θ_i represents a surface unit site containing species i. The equilibrium constant is

$$K_{HEC-FHEC} = \frac{k_{ex}}{k'_{ex}} = \left[\frac{\Gamma_{HEC}\, C_{FHEC}}{\Gamma_{FHEC}\, C_{HEC}}\right]_{equilibrium}. \qquad [3]$$

The second equality involves the bulk concentrations of the labeled and unlabeled chains, C_{FHEC} and C_{HEC}, and their surface coverages, Γ_{FHEC} and Γ_{HEC}. During self-exchange, the total adsorbed amount will be fixed if the labeled and unlabeled species are nearly identical, such that

$$\Gamma_{FHEC} + \Gamma_{HEC} = \text{ constant.} \qquad [4]$$

The exchange kinetics on the surface follow from Eq. [2]:

$$-\frac{d\Gamma_{FHEC}}{dt} = \frac{d\Gamma_{HEC}}{dt} = k_{ex}\Gamma_{FHEC}C^*_{HEC} - k'_{ex}\Gamma_{HEC}C^*_{FHEC}. \qquad [5]$$

Here C^*_{FHEC} and C^*_{HEC} are the local concentrations of the labeled and unlabeled polymer in the solution near the surface, in contrast to the bulk solution concentrations, C_{FHEC} and C_{HEC}. The local and bulk solution concentrations are related by the flux of the labeled and unlabeled species to and from the interface, J_{FHEC} and J_{HEC}, respectively.

$$J_{FHEC} = M(C_{FHEC} - C^*_{FHEC}) \qquad [6a]$$

$$J_{HEC} = M(C_{HEC} - C^*_{HEC}). \qquad [6b]$$

For shearing flow through a slit cell, the mass transfer coefficient is $M = 0.538(\gamma/L)^{1/3}D^{2/3}$. The fluxes must be equal to the amounts of labeled and unlabeled polymer adsorbed or released in the surface exchange reaction in Eq. [4]. Setting up this equality, $J_{FHEC} = -J_{HEC} = d\Gamma_{FHEC}/dt = -d\Gamma_{HEC}/dt$, the local

concentrations, C_i^*, are eliminated to yield an expression for the evolving surface concentration of labeled species:

$$\frac{d\Gamma_{\mathrm{FHEC}}}{dt} = \frac{M(\Gamma_{\mathrm{HEC}}C_{\mathrm{FHEC}} - \Gamma_{\mathrm{FHEC}}C_{\mathrm{HEC}}/K_{\mathrm{FHEC-HEC}})}{\frac{M}{k_{\mathrm{ex}}} + \Gamma_{\mathrm{HEC}} + \frac{\Gamma_{\mathrm{FHEC}}}{K_{\mathrm{FHEC-HEC}}}}. \quad [7]$$

During self-exchange studies in which unlabeled chains displace labeled ones, the bulk solution contains only HEC, and C_{FHEC} vanishes. C_{HEC} is maintained constant by flow through the cell. An equation, analogous to [7] but with the subscripts swapped, describes the evolution of Γ_{HEC}.

To interpret self-exchange runs, it is convenient to represent data in terms of the evolving surface composition, for instance $F_{\mathrm{FHEC}} = \Gamma_{\mathrm{FHEC}}/(\Gamma_{\mathrm{FHEC}} + \Gamma_{\mathrm{HEC}})$. With the constraint of constant surface coverage in Eq. [3], Eq. [7] can be integrated to yield

$$\tau = -\left(\frac{1}{\lambda} + \frac{1}{K_{\mathrm{HEC-FHEC}}}\right)\ln\left(\frac{F_{\mathrm{FHEC}}}{F^0_{\mathrm{FHEC}}}\right) + \left(1 - \frac{1}{K_{\mathrm{HEC-FHEC}}}\right)\left(F^0_{\mathrm{FHEC}} - F_{\mathrm{FHEC}}\right). \quad [8]$$

This result is implicit in the experimentally measurable quantity, F_{FHEC}, with F^0_{FHEC} being the initial fraction of labeled chains on the surface. F^0_{FHEC} is unity in our experiments. τ, which is actually the independent variable in our experiments, is the dimensionless time:

$$\tau = \frac{MC_{\mathrm{HEC}}}{\Gamma_{\mathrm{FHEC}} + \Gamma_{\mathrm{HEC}}}t. \quad [9]$$

$\tau = 0$ at the start of the self-exchange process, regardless of the layer age at that instant. Also, in Eq. [8], the dimensionless number, λ, represents the relative rates of the fundamental surface exchange process and the diffusion normal to the surface:

$$\lambda = \frac{k_{\mathrm{ex}}(\Gamma_{\mathrm{FHEC}} + \Gamma_{\mathrm{HEC}})}{M}. \quad [10]$$

As λ approaches ∞, the fundamental surface rate exceeds the rate of diffusion toward the surface, and the observed exchange process becomes transport-limited.

With true self-exchange, fluorescent tags act only as tracers such that the labeled and unlabeled species are identical. Then, $k_{\mathrm{ex}} = k'_{\mathrm{ex}}$, and $K_{\mathrm{HEC-FHEC}} = K_{\mathrm{FHEC-HEC}} = 1$. This assumption is frequently violated, for instance, with deuterio and protiopolystryene adsorbing on silica from CCl_4 (40), and fluorescein-tagged PEO adsorbing onto silica at low ionic strengths (41). For coumarin tagged (PEO) on silica, the label was minimally invasive, with $K_{\mathrm{CPEO-PEO}} = 2.5$ for molecular weights near 100,000 (10).

Values of $K_{\mathrm{HEC-FHEC}}$ were sought for the current investigation by extracting partitioning information from runs like those in Fig. 2b but where the labeled fraction in the bulk solution was varied. This approach is difficult because relaxations influence fluorescence, leading to a worst-case estimate of $K_{\mathrm{HEC-FHEC}}$, in

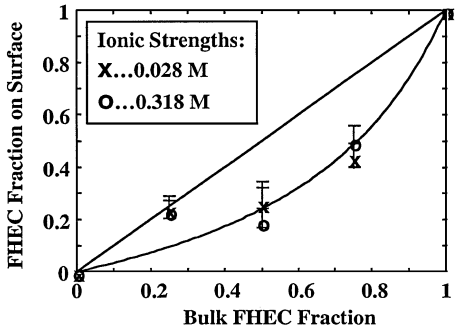

FIG. 4. Worst case binary partitioning diagram for binary solutions of FHEC and HEC, with a total polymer concentration of 100 ppm. The curve is Eq. [3] for a $K_{\mathrm{HEC-FHEC}}$ value of 3.2.

Fig. 4. In this case the equilibrium curve through the data, per Eq. [3], corresponds to $K_{\mathrm{HEC-FHEC}} = 3.2$, suggesting that fluorescein tagging might be slightly invasive, with unlabeled chains being favored over labeled ones on the surface. This would correspond to a worst-case estimated energy difference of 1.16 kT per chain.

The data used to obtain $K_{\mathrm{HEC-FHEC}} = 3.2$ were runs like Fig. 2b, where it was assumed that the decay process is due exclusively to displacement of labeled species by native HEC, which we know is not occurring for several reasons. The first is that the decay during FHEC adsorption persists when buffer solution water is flushed over the layer. In cases where the decay was due to displacement of labeled chains by unlabeled chains as part of the adsorption process, the decay was interrupted when DI water was injected (42). Second, in cases where the adsorption of unlabeled material was preferred over fluorescein-labeled material, the effect was ionic strength dependent (40). Figure 4 shows that over the ionic strength range from 0.02 to 0.3 M, there is negligible influence of ionic strength. Based on these arguments, we proceed with the interpretation that the primary reason for the decay prior to the initiation of self-exchange is interfacial relaxations.

Another perspective on the potential invasiveness of the fluorescein label derives from a comparison of the forward and reverse self-exchange kinetics, shown in Fig. 5. In this study two runs are compared: In the first, FHEC is adsorbed for 120 min, exposed to flowing buffer for 60 min, and then challenged with unlabeled HEC. In the second, unlabeled HEC is adsorbed for 120 min, exposed to flowing buffer for 60 min, and then challenged with FHEC. Figure 5 shows only the exchange processes following the initial adsorption and layer aging. If the fluorescein tag is noninvasive, per a true self-exchange run, then the two curves will be exact mirror images of each other (10). As the fluorescein labeling becomes invasive, with the unlabeled material being preferred on the surface over the adsorbed material, the curves become skewed, per the calculations, in Fig. 5b.

The symmetry between the two runs in Fig. 5a suggests minimal invasiveness of the fluorescein tag, whose repulsion from the negative silica surface is screened at ionic strengths in this work. The displacement of unlabeled chains by labeled ones is

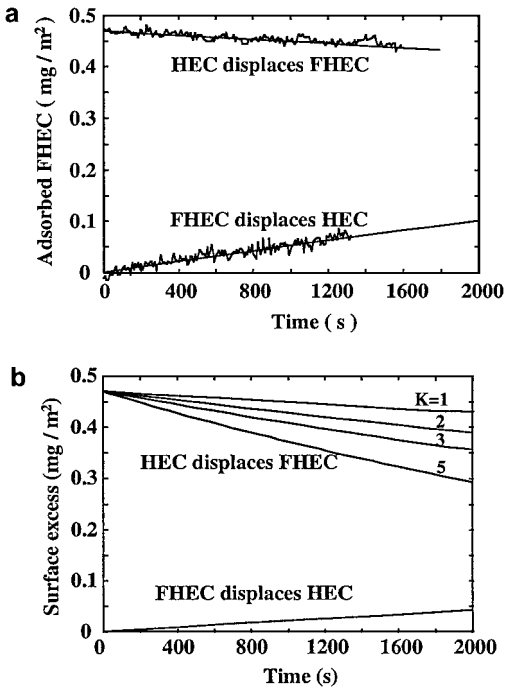

FIG. 5. (a) Forward and reverse self-exchange of HEC in 3-h-old layers. Line is best fit to Eq. [8] with $\lambda = 0.0015$ and $K_{\mathrm{HEC-FHEC}} = 0.88$. (b) Expected self-exchange traces for different values of surface preference for labeled chains: $K_{\mathrm{HEC-FHEC}}$ varies as shown by varying k_{ex} and fixing k'_{ex}. Note that when k_{ex} varies, so does λ per the definition in Eq. [10]. In (b), $\lambda = 0.0015$ when $K_{\mathrm{HEC-FHEC}} = 1$.

only slightly faster than the reverse, with $K_{\mathrm{HEC-FHEC}} = 0.88$, corresponding to a ΔG_{ex} of 0.1 kT.

Since the fluorescein labeling of HEC has been shown to be minimally invasive, it is possible to simplify Eq. [8], if we approximate $K_{\mathrm{FHEC-HEC}} \sim K_{\mathrm{HEC-FHEC}} \sim 1$. Then Eq. [8] becomes

$$F_{\mathrm{FHEC}} = \exp\left(-\frac{ct}{1+\frac{1}{\lambda}}\right). \qquad [11]$$

Here c is a constant equal to 0.311 under our experimental conditions. Equation [11] shows that in the limit of perfect self-exchange with a first-order surface kinetic constant, an exponential decay should result for the decrease in the surface fluorescence. Such exponential decays were sometimes found for the initial kinetics in previous studies such as the displacement of protiopolystyrene on silica by deuteriopolystyrene (11) and the displacement of polystyrene by deuterio-*cis*-polyisoprene at elevated temperatures (14). In these cases the exponential decay was interpreted to mean that conditions were such that local equilibrium was achieved and that a simple forward irreversible exchange rate dominated the behavior (13). The previous interpretation did not take into account the surface preference for the incoming species, which was substantial in those studies and would, according to our treatment in Eq. [8] (and our previous works) (10), cause deviations from exponential behavior. Further, Eq. [11] predicts that when the surface has minimal preference for the initially adsorbed or invading polymer, exponential decays are expected for a wide range of λ values. In other words, it is possible to observe exponential decays with transport-limited kinetics, first-order surface-limited kinetics, or conditions between these two limiting cases. This finding contrasts with previous ideas about self-exchange where an exponential decay is a limiting equilibrium behavior (13). Further, in our work, reversible exchange is a necessary condition to reach Eq. [11]. In prior interpretations of polymer exchange studies, the surface step was frequently treated as unidirectional (13), even though there were no fundamental experimental constraints that would prevent reversibility.

Figure 6 shows a series of self-exchange experiments in which HEC displaces FHEC layers of increasing ages. All bulk solution concentrations are 100 ppm, contributing to the early fluorescence signal. In these experiments, FHEC was allowed to adsorb for 10 min, aged under flowing buffer to different extents, and then challenged with unlabeled HEC. The displacement of the FHEC from the surface by HEC was then tracked. Notably, during self-exchange when the HEC was injected, there was no overshoot in the total mass (checked separately with reflectivity, which is not shown here). Overshoots were sometimes seen by other investigators with systems having preference for the invading species (13–15). Instead, we observed a slight increase

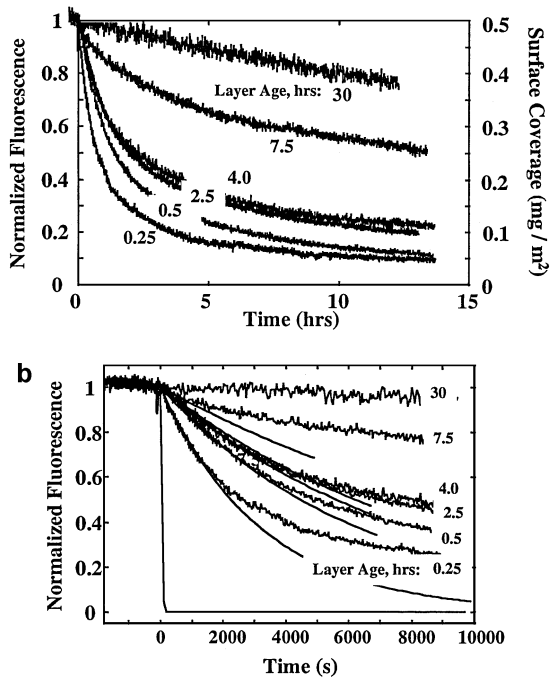

FIG. 6. (a) The effect of adsorbed layer age on self-exchange kinetics as seen by TIRF. Each layer has been aged for increasing periods prior to the onset of self-exchange (time zero), as labeled. (b) Comparison of short time data to Eq. [11]. Each data set and the corresponding curve for Eq. [11] are matched at short times. Equation [11] is not shown for the 30-h-old layer, as the observed decay is horizontal. The sharply dropping curve represents the transport limited case for $\lambda = \infty$.

in the total coverage, commensurate with that in Fig. 2a. The coverage increases slightly because the equilibrium coverage with polymer in the bulk solutions of 100 ppm is slightly higher than that when the bulk solutions are dilute (during aging), on the order of a fraction of a ppm.

In Fig. 6a, all the runs are normalized to $F_0 = 1$ at the start of self-exchange. The kinetic traces illustrate that self-exchange is more extensive for young layers than for layers that have aged substantially. For layers aged 30 h, detecting any self-exchange at all in a 10 h period was difficult. Only the persistent fluorescent decay, resulting from changes in quantum yield, signaled continuing changes in the layer beyond 30 h of aging. Figure 6b shows a close-up of the short time decay behavior, corrected for the underlying fluorescence decay (determined from the 30 h aging run), with the best fit to Eq. [11] included for each data set. For young layers, the single exponential decay describes a substantial fraction, up to 30%, of the initially adsorbed polymer. For older layers, the single exponential decay is a poor approximation to the data, allowing us only to identify an initial limiting slope as a rough measure of the state of the layer. In all cases, the exchange is self-retarding, with some of the original chains remaining on the surface hours after the exchange was initiated. The retardation of the self-exchange is expected, since in long self-exchange runs, the layer ages as the exchange proceeds.

In addition to the single exponential form in Eq. [11], we attempted to fit the experimental decays to stretched exponential per the procedure of Granick (11–15). The stretched exponential fits were extremely poor, as shown by the example in Fig. 7. Though the stretched exponential form appears to accommodate most of the data, one should recall that a stretched exponential must exhibit a good fit over several decades in time. Our data only approximate stretched exponential behavior over 1 decade (from 3 to 20 h), arguing that this form is not an accurate description of our results. Notably, previous studies with PEO self-exchange were also not well described by stretched exponential decays (10).

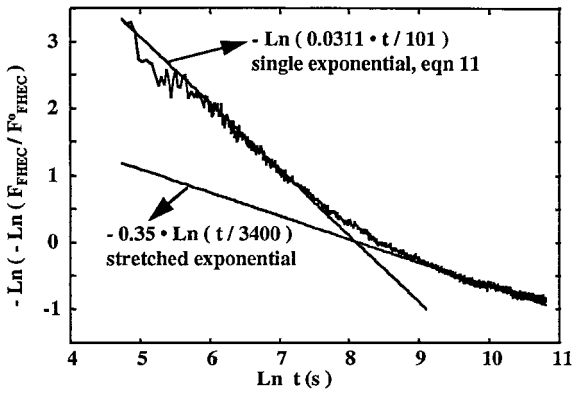

FIG. 7. Test of stretched exponential fit to data from Fig. 6 for exchange in an 0.25-h-old layer. The two straight lines represent a single exponential fit to the short time data and a stretched exponential fit (with a stretching exponent of 0.35) to the long time data.

We also attempted to fit the data to the sum of two exponentials. This form may have physical significance for bimodal relaxations, for instance, a main cellulose backbone relaxation and a secondary side ethylene oxide oligomer relaxation. While the data could be forced fit to this form, the analysis was ambiguous and therefore not continued. We would have liked several decades of data to establish the fit to each of the two exponentials, which was not available. Therefore, the crossover and the two time constants were poorly defined. If future theoretical developments argue strongly in favor of the biexponential form, we could extract decay scales from our data. The current data, by themselves, do not, however, justify such a form.

Because the results in Fig. 6 do not easily lend themselves to further quantitative analysis, at this stage we summarize, in Fig. 8, the different measures of HEC layer evolution during incubation in solvent and make comparisons to other systems where possible. Figure 8a summarizes the k_{ex} constants extracted from the λ values in Eq. [11], and makes comparisons with PEO. Figure 8b summarizes the long-time fluorescent decays, and Fig. 8c shows the retained coverage from the originally adsorbed FHEC layer after 10 h of self-exchange. Figures 8a and 8c indicate that the layer becomes immobile to exchange with the bulk solution by approximately 30 h; however, Fig. 8b indicates that even after chains become immobilized, the fluorescence continues to decay, suggesting local segmental rearrangmenets within the layer.

In Fig. 8a, the surface-exchange rate constants for HEC are at least 2 orders of magnitude slower than those of PEO, especially for the young layers. This may be due to HEC's stiffer backbone, since the segment–surface interactions for HEC or PEO on silica are similar (polymer ether oxygen hydrogen bonding with surface silanol.) Also in Fig. 8a, the k_{ex} values decrease with layer age and for HEC, the evolution of k_{ex} was fit to the form $\exp((-0.4\,\mathrm{h}^{-1}\,t(\mathrm{h}))^{0.3})$. This stretched exponential form roughly fits the observed evolution of k_{ex} at short times but failed to fit the complete evolution of k_{ex}. For 120K PEO, however, the form $k_{ex} = \exp[-0.7\ \mathrm{h}^{-1}\ t(\mathrm{h})]$ gave an adequate fit for the evolution of k_{ex}. The fit was sufficient even at long times, which is not evident on the particular y-axis scaling in Fig. 8a. Of note for HEC in Fig. 8a, there is no evidence for bimodal layer evolution kinetics. This suggests that the main stiff HEC backbone dominates the relaxations and that contributions of short EO side chains are too fast to observe.

One of the remarkable features of the results in Figs. 6–8 is the qualitative similarity between the polydisperse HEC and the narrow molecular weight standard 120K PEO in our previous study (10). For both systems highly mobile layers evolve, over a period of $\sim$20 h, to a state that has no self-exchangeable populations. The similarity of the relaxation times (15–25 h) comes as a surprise in light of the molecular weight sensitivity of relaxations in adsorbed layers. For PEO and HEC, we do, however, observe important differences in the self-exchange kinetics of young layers with similar adsorption histories. These differences are attributed to the backbone flexibility.

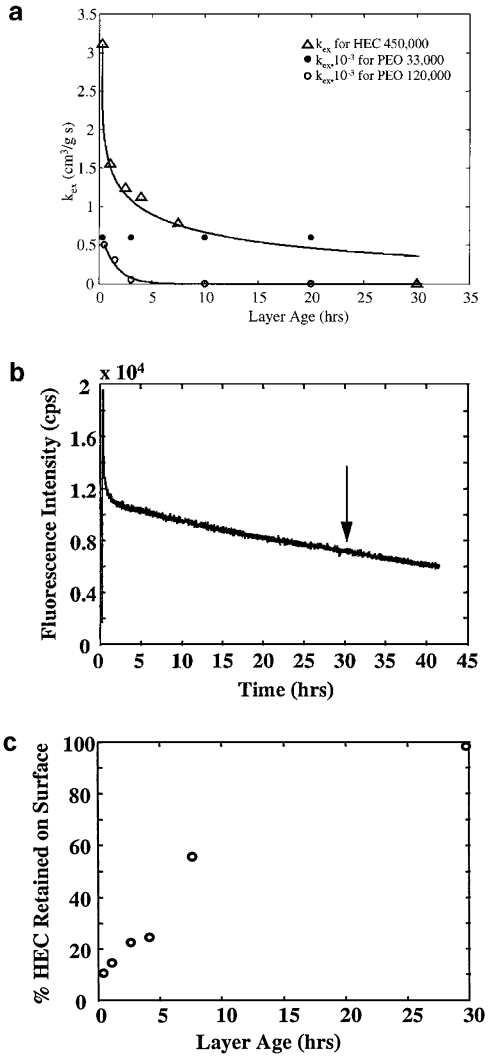

FIG. 8. (a) Values of k_{ex} obtained by fitting the early parts of HEC self-exchange to Eq. [11]. Circular symbols facilitate a comparison with PEO relaxations in similar aging and self-exchange studies. Note that PEO data are reduced by a factor of 1000 to fit them on the same figure with the HEC data. The curve through the HEC data is the best stretched exponential fit. The curve through the 120K PEO data is the best exponential decay. (b) Long runs showing extensive fluorescent decay. Injection of unlabeled HEC at 30 h (arrow) does not affect decay behavior, signaling no self-exchange. The rapid signal drop at 15 min results form injection of solvent. (c) Percentage of retained FHEC after 10 h of self-exchange, as a function of layer age.

Though the effects of polydispersity were not obvious in our study, polydispersity would cause the average molecular weight within the adsorbed layer to increase as exchange proceeded, causing the self-exchange to retard to a greater extent than it would in monodisperse systems. This may cause the aging and immobilization of the layer to appear accelerated. In the current study, we took precautions to avoid polydispersity effects in the short time data by having short initial adsorption times prior to aging in pure flowing solvent. By aging the layer in solvent rather than in polydisperse polymer solution, the molecular weight in the layer is held near that of the bulk solution, so that at the start of self-exchange the bulk and interface have the same molecular weight distributions. If the initially adsorbed layer were higher in molecular weight than the solution (which could result from aging in the labeled solution rather than solvent), then the initial exchange would be artificially slow. Our initial HEC self-exchange rates are much slower than those observed for PEO. Therefore the relative k_{ex} values are attributed to HEC's backbone stiffness rather than polydispersity.

As a final note, we hesitate to report equilibration times for the HEC layers in the current work. While HEC layers were no longer susceptible to self-exchange after about 25 h of aging in flowing solvent, the continued fluorescent evolution (in Fig. 8b) suggested further relaxations beyond those measurable through self-exchange. If one compares the evolution of the layer's dynamic exchangeability, in Fig. 8a, to its evolving structure, signaled by the fluorescence decay (which translates in a complicated way to loop size distribution) one observes very different decay shapes and time scales. The former is stretched exponentially while the latter is more nearly linear and signals layer evolution even at 30 h.

CONCLUSIONS

This work probed the adsorption kinetics of HEC layers on silica and, through self-exchange and steady-state fluorescence, the evolving dynamic state of the adsorbed layer. Adsorption kinetics were shown to be transport-limited, with a rounded shoulder characteristic of polydisperse samples. Desorption was slow, in keeping with expectations for systems having adsorption isotherms with flat plateaus down to extremely dilute bulk solution concentrations. Initially adsorbed HEC layers were highly mobile, exhibiting self-exchange between the bulk solution and the adsorbed layer that involved almost all of the initially adsorbed chains for young layers. With increasing layer age up to 30 h, the self-exchange became hindered, and ultimately none of the originally adsorbed chains were able to exchange with those in the bulk solution. A continued fluorescent evolution signaled continued changes in the adsorbed layers, beyond time scales that could be probed through self-exchange.

Continued incubation in the original polymer solution (as opposed to solvent only) accelerated the apparent aging rate of the layer through the exchange between high- and low-molecular-weight populations ultimately increasing the interfacial molecular weight. Layers whose average molecular weight was elevated through initial self-exchange in the adsorption solution were more difficult to displace in tracer self-exchange studies because the lower molecular weight chains in the bulk solution are, for thermodynamic reasons, ineffective at displacing the higher molecular weight chains on the surface. This phenomenon can cause adsorbed layers to appear more immobile than they really are and will also be a self-retarding factor in any self-exchange study with a polydisperse sample.

Despite the complexities arising from polydispersity in HEC samples, the self-exchange rate constants for HEC were over

an order of magnitude slower than those of PEO, signaling that other factors besides polydispersity are important. (Polydispersity will tend to cause a tailing of the self-exchange kinetics.) Since the segment–surface interactions for HEC and PEO on silica are very similar, it is most likely that dynamic differences in the two systems resulted from differences in backbone stiffness, with the bulky sugar rings of HEC hindering its motion. Interestingly, self-exchange kinetics for both HEC and the previously studied PEO were neither exponential nor stretched exponential. The evolution, during layer aging in solvent, of the surface-exchange rate constant did, however, adhere to a stretched exponential form.

ACKNOWLEDGMENT

This work was supported by the National Science Foundation, CTS–9817048.

REFERENCES

1. Lee, J. J., and Fuller, G. J., *Macromolecules* **17,** 375 (1984).
2. Pefferkorn, E., Carroy, A., and Varoqui, R., *J. Polym. Sci. Part B* **23,** 1997 (1985).
3. Scheutjens, J. M. H. M., Fleer, G. J., and Cohen Stuart, M. A., *Colloids Surf.* **21,** 285 (1986).
4. Scheutjens, J. M. H. M., and Fleer, G. J., *Macromolecules* **18,** 1882 (1985).
5. Scheutjens, J. M. H. M., and Fleer, G. J., *Adv. Colloid Interface Sci.* **16,** 361 (1982).
6. Klein, J., and Luckham, P., *Macromolecules* **17,** 1041 (1984).
7. Chang, M.-C., Lin, H.-L., Huang, C.-L., Wang, Y.-Y., and Wan, C.-C., *Colloids Surf. A: Physio. Eng. Asp.* **139,** 75 (1998).
8. Santore, M. M., Russel, W. B., and Prud'homme, R. K., *Faraday Discus. Chem. Soc.* **90,** 323 (1990).
9. Soga, I., and Granick, S., *Macromolecules* **31,** 5450 (1998).
10. Fu, Z., and Santore, M. M., *Macromolecules* **32,** 1939 (1999).
11. Frantz, P., and Granick, S., *Phys. Rev. Lett.* **66,** 899 (1991).
12. Frantz, P., and Granick, S., *Macromolecules* **27,** 899 (1991).
13. Douglas, J., Frantz, P., Johnson, H. E., Schneider, H. M., and Granick, S., *Colloids Surf. A: Physio. Eng. Asp.* **86,** 251 (1994).
14. Schneider, H. M., Granick, S., and Smith, S., *Macromolecules* **27,** 4721 (1994).
15. Schneider, H. M., Granick, S., and Smith, S., *Macromolecules* **27,** 4714 (1994).
16. Brandup, J., Immergut, E. H., "Polymer Handbook," 2nd ed. Wiley, New York, 1975.
17. Elias, H. G., "Macromolecules 1, Structure and Properties," 2nd ed. Plenum, New York, 1984.
18. Fu, Z., Ph.D. thesis, Polymer Science and Engineering Program, p. 26, Lehigh University, 1998.
19. van der Beek, G. P., and Cohen Stuart, M. A., *Langmuir* **7,** 327 (1991).
20. Cohen Stuart, M. A., Fleer, G. J., Scheutjens, *J. Colloid Interface Sci.* **97,** 526 (1984).
21. Chen, C. H., Wilson, J. E., Davis, R. M., Chen, W., and Riffle, J. S., *Macromolecules* **27,** 6376 (1994).
22. Private communication from Professor J. E. Glass, University of North Dakota.
23. Kaczmarski, J. P., Tarng, M.-R., Glass, J. E., and Buchacek, R. J., *Prog. Org. Coatings* **30,** 15 (1997).
24. Tadros, Th. F., *J. Colloid Interface Sci.* **64,** 36 (1978).
25. Fu, Z., and Santore, M. M., *Colloids Surf. A: Physio. Eng. Asp.* **135,** 63 (1998).
26. Brown, W. *Arkiv For Kemi.* **18**(16), 227 (1961).
27. Rebar, V. A., and Santore, M. M., *J. Colloid Interface Sci.* **178,** 29 (1996).
28. Kelly, M. S., and Santore, M. M., *Colloids Surf. A: Physio. Eng. Asp.* **96,** 199 (1995).
29. Rebar, V. A., and Santore, M. M., *Macromolecules* **29,** 6263 (1996).
30. Fleer, G. J., Cohen Stuart, M. A., Scheutjens, J. M. H. M., Cosgrove, T., and Vincent, B., "Polymers at Interfaces," Chapman and Hall, London, 1993.
31. Scheutjens, J. M. H. M., and Fleer, G. J., *J. Phys. Chem.* **83,** 1619 (1979).
32. Cohen Stuart, M. A., Cosgrove, T., and Vincent, B., *Adv. Colloid Interface Sci.* **24,** 143 (1986).
33. Kelly, M. S., and Santore, M. M., *J. Appl. Polym. Sci.* **58,** 247 (1995).
34. Khoultchaev, K. K., Kerekes, R. J., and Englezos, P., *AICHE J.* **43,** 2553 (1997).
35. Dijt, J. C., Cohen Stuart, M. A., and Fleer, G. J., *Macromolecules* **25,** 5416 (1992).
36. Leveque, M., *Ann. Mines* **13,** 284 (1928).
37. Santore, M. M., Kelly, M. S., Mubarekyan, E., and Rebar, V. X., *in* "Surfactant Adsorption and Surface Solubilization" (R. Sharma, Ed.), Ch. 11, ACS Symposium Series 615, American Chemical Society, Washington, DC, 1995.
38. Lok, B. K., Cheng, Y., and Robertson, C. R., *J. Colloid Interface Sci.* **91,** 104 (1983).
39. Robeson, J. L., and Tilton, R. D., *Biophys. J.* **68,** 2145 (1995).
40. Schneider, H. M., and Granick, S., *Macromolecules* **26,** 5054 (1992).
41. Fu, Z., and Santore, M. M., *Langmuir* **14,** 4300 (1998).
42. Rebar, V. A., and Santore, M. M., *Macromolecules* **29,** 6273 (1996).